Body Flexibility Effects on Foot Loading in Quadruped Bounding Based on a Simple Analytical Model

Tomoya Kamimura, Shinya Aoi, Kazuo Tsuchiya, and Fumitoshi Matsuno

***Abstract*—Body flexibility plays an important role in the bounding gait of quadruped animals. In a previous study, we investigated the effects of body flexibility on foot loading by comparing two different physical models, with and without a flexible body-joint. Testing both models with equal mechanical energy revealed two conflicting results: Body flexibility reduced the maximum ground reaction force, but a stiffer body exhibited a smaller maximum ground reaction force than a highly flexible body. Because of the complex nature of the model dynamics, the mechanisms underlying these results are unclear. In the current study, we used a simplified analytical model by assuming physical constraints on our previous model to clarify the dynamic roles of body flexibility, particularly regarding foot loading. Approximate periodic solutions were derived by linearization of the governing equations and provide an explanation for our conflicting results. Furthermore, we discussed the biological relevance of our findings using a comparison of our analytical results with observations of movement in cheetahs. Our findings will not only improve the understanding of motor control mechanisms for fast locomotion in quadruped animals, but also provide a guiding principle for the mechanical and control design of legged robots capable of fast locomotion.**

***Index Terms*—Biologically-inspired robots, legged robots, flexible robots.**

I. Introduction

QUADRUPED animals, such as cheetahs, use body flexibility for fast locomotion. Hildebrand [1], [2] observed fast running in cheetahs, reporting that they exhibited remarkable flexibility, extending the spine to increase stride length by swinging the limbs further to enhance speed. However, quadruped running is governed by two different dynamics in the flight phase and stance phase. During the flight phase, all feet are in the air and the center of mass (COM) of the whole body exhibits ballistic motion. In contrast, during the stance phase, some of the feet are in contact with the ground and the legs behave like springs. Because of the complex and hybrid nature of the governing dynamics, there are limitations to the understanding of the role of body flexibility in quadruped running that can be gained from observations of animals alone.

To overcome the limitations of the observational approach, modeling approaches have attracted recent research attention. Alexander [3] used a simple dynamical model and suggested that quadruped running is energetically efficient because energy is stored in elastic elements of the body then released. Because the essential contribution of the legs can be represented by springs, the spring-loaded inverted pendulum (SLIP) model was developed to investigate animal locomotion mechanisms from a dynamic viewpoint, especially for human running [4]–[6]. The SLIP model has been revised to enable investigation of human walking [7], [8], explaining the dynamic essence for different patterns of vertical ground reaction force (GRF) between human walking and running. Furthermore, the SLIP model has been used for examining gait in other animals including quadrupeds, to clarify the common and unique principles between animal gaits [9]–[12]. The SLIP model also has been used for quadruped robots [13]–[17]. In particular, Poulakakis *et al.* [14] developed a quadruped robot called Scout II that exhibited stable bounding gait. In addition, the researchers demonstrated that a simple two-legged SLIP-based model captured the dynamical features of the bounding gait of the robot and clarified the parameter region for stable bounding gait [15].

Recently, the SLIP model has been further developed to investigate the dynamic roles of body flexibility in quadruped running. Cao and Poulakakis introduced a passive springy joint in the trunk and investigated the stability characteristics [18] and energy efficiency [19] during bounding gait. These results showed that introducing such a joint in the trunk allowed the model to capture dynamical features of the bounding gait with body flexibility. Yamasaki *et al.* [20] incorporated a passive spine joint with a rotational spring and a damper, achieving a periodic bounding gait with a stable limit cycle. Pouya *et al.* [21] reported that a model with a passive spine joint achieved a more energy-efficient gait than a model with an active spine joint. Wang *et al.* [22] used four springy legs as well as a passive spine joint and found a stable rotary galloping gait.

GRF has been suggested as an important factor for evaluating dynamic locomotor mechanisms in fast quadruped running [23]. This factor is also crucial for legged robots in fast locomotion to

Manuscript received February 23, 2018; accepted May 15, 2018. Date of publication June 1, 2018; date of current version June 22, 2018. This letter was recommended for publication by Associate Editor H. Hu and Editor Y. Sun upon evaluation of the reviewers' comments. This work was supported in part by the Grant-in-Aid for Young Scientists (A) 17H04914 from the Ministry of Education, Culture, Sports, Science, and Technology (MEXT) of Japan. *(Corresponding author: Tomoya Kamimura.)*

T. Kamimura and F. Matsuno are with the Department of Mechanical Engineering and Science, Graduate School of Engineering, Kyoto University, Kyoto 615-8540, Japan (e-mail: kamimura.tomoya.77s@st.kyoto-u.ac.jp; matsuno.fumitoshi.8n@kyoto-u.ac.jp).

S. Aoi and K. Tsuchiya are with the Department of Aeronautics and Astronautics, Graduate School of Engineering, Kyoto University, Kyoto 615-8540, Japan (e-mail: shinya_aoi@kuaero.kyoto-u.ac.jp; tsuchiya_k@nifty.com).

Digital Object Identifier 10.1109/LRA.2018.2842925

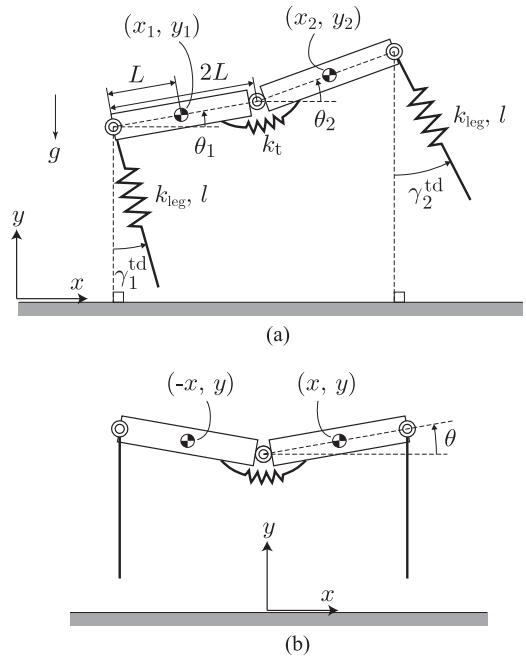

Fig. 1. (a) Bounding gait model with a flexible body joint and parameter definition. (b) Simplified model by constraint of movement (flexible body model).

avoid damage. Therefore, it is important to clarify the features of GRF in quadruped running. In our previous study [24], we investigated the relationship between body flexibility and GRF during bounding gait by comparing two different quadruped models, one of which had a flexible body joint and the other of which did not. The results revealed that the maximum GRF of the model with body flexibility was lower than that of the model without body flexibility when their mechanical energies were identical, suggesting that body flexibility reduces maximum GRF. However, the results also indicated that maximum GRF increased as joint stiffness decreased, suggesting that body flexibility increased maximum GRF. The mechanisms underlying these conflicting results are currently unclear, mainly because of the complexity of the models. In the current paper, we used a simplified analytical model by assuming some physical constraints on our previous model and derived approximate periodic solutions to clarify the mechanisms underlying these conflicting results. Furthermore, we discuss the biological relevance of our findings for periodic bounding gait, and propose some guiding principles for the mechanical and control design of legged robots based on analytical solutions.

II. Model

A. Bounding Gait Model With a Flexible Body Joint

In the current paper, to investigate the contribution of body flexibility in bounding gait reported as in previous studies [18]–[22], we used a physical model consisting of two rigid bodies connected by a torsional spring joint (torsional spring constant: k_t) and two massless springs for the legs (Fig. 1(a)), as used in [24]. Because the torsional spring constant k_t determines the body flexibility, we investigated gait characteristics using k_t.

This model is constrained in two dimensions. x_1 and y_1 are, respectively, the horizontal and vertical positions of the hind body (x_2 and y_2 are those of the fore body). θ_1 and θ_2 are, respectively, the pitch angles of the hind and fore bodies relative to the horizontal line. We assumed that the fore and hind parts of the model have the same physical parameters. The mass and the moment of inertia around the COM of the bodies are m and J, respectively. The length of the bodies is $2L$. The distance between the COM and the root of the leg spring is L. The spring constant and the neutral length of the massless legs are k_{leg} and l, respectively. The torsional spring is at the equilibrium position when the fore and hind bodies are in a straight line ($\theta_1 = \theta_2$). g is the gravitational acceleration. During the swing phase, the spring length remains l and the angle relative to the vertical line keeps the specific value γ_1^{td} for the hind leg and γ_2^{td} for the fore leg, which corresponds to the touchdown angle. During the stance phase, the spring length and the angle relative to the vertical line are determined by $x_1, y_1, \theta_1, \theta_2$, and the touchdown position. Because the touchdown and liftoff occur at the neutral length, the physical system is energy conservative.

We determined the physical parameters of the model as follows: $m = 18.4$ kg, $J = 0.18$ kgm^2, $L = 0.19$ m, and $l = 0.57$ m, based on measured data from cheetahs by Hudson *et al.* [25], and $k_{leg} = 8000$ N/m based on Farley *et al.* [11] (k_{leg} is used in Section IV-C).

B. Constraint of Movement and Governing Equations

To clarify the dynamic characteristics of quadruped bounding, we focused on a specific movement of the model, in which the motions of the fore and hind parts of the model are symmetrical, and touchdown and liftoff of the fore and hind legs occur simultaneously using $\gamma_1^{td} = \gamma_2^{td} = 0$ as shown in Fig. 1(b). In this case, the COM of the model moves only vertically. Under this constraint, the state variables are redefined by $x_1 = -x_2 \equiv -x$, $y_1 = y_2 \equiv y$, and $\theta_1 = -\theta_2 \equiv -\theta$. In addition, $x = L\cos\theta$ is satisfied.

During the flight phase, the equations of motion of the model are obtained from the Lagrangian equation (Lagrangian $\mathcal{L}$ is given by $\mathcal{L} = m(L^2\dot{\theta}^2\sin^2\theta + \dot{y}^2) + J\dot{\theta}^2 - 2mgy - 2k_t\theta^2$) by

$$2m\ddot{y} = -2mg, \tag{1a}$$

$$(2mL^2\sin^2\theta + 2J)\ddot{\theta} = -4k_t\theta - mL^2\dot{\theta}^2\sin 2\theta. \tag{1b}$$

When the swing leg lands on the ground, the phase of the model shifts from the flight phase to the stance phase. For $\boldsymbol{q} = [y\ \theta\ \dot{y}\ \dot{\theta}]^\top$, the geometric condition of the foot contact (the contact condition) is given by

$$r(\boldsymbol{q}^-) = l - y^- - L\sin\theta^- = 0, \tag{2}$$

where $*^-$ indicates the state immediately prior to foot contact.

The duty factor in quadruped galloping is small (e.g., approximately 0.12 to 0.26 in cheetahs [25]). We assumed that the stance phase is sufficiently short and that the foot contact can be regarded as an elastic collision, involving no position

change and energy conservation. Because of the constraints of the movement, the current model only receives the impulsive force from the ground vertically. The relationship between the states immediately prior to and immediately following the collision is given by

$$\dot{y}^+ = -\frac{J - mL^2\cos^2\theta^-}{J + mL^2\cos^2\theta^-}\dot{y}^- - \frac{2JL\cos\theta^-}{J + mL^2\cos^2\theta^-}\dot{\theta}^-, \quad (3a)$$

$$\dot{\theta}^+ = -\frac{2mL\cos\theta^-}{J + mL^2\cos^2\theta^-}\dot{y}^- + \frac{J - mL^2\cos^2\theta^-}{J + mL^2\cos^2\theta^-}\dot{\theta}^-, \quad (3b)$$

where $*^+$ indicates the state immediately following the collision. The derivation of these equations is presented in the Appendix.

C. Linearization of Governing Equations

We speculated that $\theta \ll 1$ and $\dot{\theta} \ll 1$. The linearization of the equations of motion (1) during the flight phase gives

$$\ddot{y} = -g, \quad (4a)$$

$$\ddot{\theta} = -\omega^2\theta, \quad (4b)$$

where $\omega = \sqrt{2k_t/J}$. The equations are separated into an equation for the ballistic motion of the COM of the whole body and an equation for simple harmonic oscillation by the torsional spring.

The contact condition (2) is approximated by

$$r(\boldsymbol{q}^-) = l - y^- - L\theta^- = 0. \quad (5)$$

The relationship between the states immediately prior to and immediately following the collision (3) is approximated by

$$\boldsymbol{q}^+ = H\boldsymbol{q}^-, \quad (6)$$

where

$$H = \begin{bmatrix} 1 & 0 & 0 & 0 \\ 0 & 1 & 0 & 0 \\ 0 & 0 & -\dfrac{J - mL^2}{J + mL^2} & -\dfrac{2JL}{J + mL^2} \\ 0 & 0 & -\dfrac{2mL}{J + mL^2} & \dfrac{J - mL^2}{J + mL^2} \end{bmatrix}. \quad (7)$$

III. Periodic Solution

A. Derivation of Approximate Periodic Solutions

In the current study, we found periodic motion with one flight phase and one collision for each gait cycle. We defined the periodic solution as $\boldsymbol{q}^*(t)$ $(0 \le t \le T)$, where $t = 0$ is the time immediately following the collision and T is the gait cycle duration. $\boldsymbol{q}^*(T)$ is the state immediately prior to the collision. (6) becomes

$$\boldsymbol{q}^*(0) = H\boldsymbol{q}^*(T). \quad (8)$$

From (4), we obtain

$$y(t) = -\frac{g}{2}t^2 + at + b, \quad (9a)$$

$$\theta(t) = A\cos(\omega t + \phi), \quad (9b)$$

where a, b, $A \ge 0$, and $-\pi \le \phi \le \pi$ are constant. The substitution of (9a) into the first and third rows of (8) gives

$$\dot{y}^*(T) = -\dot{y}^*(0), \quad (10a)$$

$$T = \frac{2\dot{y}^*(0)}{g}. \quad (10b)$$

From (10a) and the third row of (8), we obtain

$$\dot{y}^*(T) = \frac{J}{mL}\dot{\theta}(T). \quad (11)$$

From (11) and the fourth row of (8), we obtain

$$\dot{\theta}^*(T) = -\dot{\theta}^*(0). \quad (12)$$

The substitution of (9b) into the second row of (8) gives

$$T = \frac{2n\pi - 2\phi}{\omega}, \quad (13)$$

where $n \ge 1$ is an arbitrary integer and ϕ is restricted to $0 \le \phi < \pi$. From (9a), (10b), and (13), we obtain

$$a = \dot{y}^*(0) = \frac{g(n\pi - \phi)}{\omega}. \quad (14)$$

By substituting (10b), (11), and (14) into (9b), we obtain

$$A = -\frac{mgL(n\pi - \phi)}{J\omega^2\sin\phi}. \quad (15)$$

From (5) and (8), we obtain $r(\boldsymbol{q}^*(0)) = 0$, which gives

$$b = \frac{mgL^2(n\pi - \phi)}{J\omega^2\tan\phi} + l. \quad (16)$$

As a result, approximate periodic solutions are obtained by

$$y^*(t) = -\frac{g}{2}t^2 + \frac{g(n\pi - \phi)}{\omega}t + \frac{mgL^2(n\pi - \phi)}{J\omega^2\tan\phi} + l, \quad 0 \le t \le T \quad (17a)$$

$$\theta^*(t) = -\frac{mgL(n\pi - \phi)}{J\omega^2\sin\phi}\cos(\omega t + \phi), \quad 0 \le t \le T \quad (17b)$$

$$T = \frac{2(n\pi - \phi)}{\omega}, \quad (17c)$$

where $n \ge 1$ is an arbitrary integer and $0 \le \phi < \pi$ is an arbitrary constant. n indicates the number of oscillations of the body spring and ϕ and $2n\pi - \phi$ are the initial $(t = 0)$ and terminal $(t = T)$ phases of the oscillations. Therefore, the phase angle changes by $2n\pi - 2\phi$ in one gait cycle. The approximate periodic solutions were obtained for arbitrary integer n as a general characteristic of the solution, as observed in a two-legged SLIP model [7]. However, $n \ge 2$ implies multiple oscillations and is unusual for animals. $n = 1$ generally corresponds to the animals' bounding.

B. Comparison of Periodic Solutions Between Approximate Analysis and Dynamic Simulation

To verify the validity of the approximate analysis, we compared the approximate solution obtained in (17) (Approx. Analy.) with the periodic solutions obtained by the numerical simulation (Num. Sim.). The numerical simulation used the

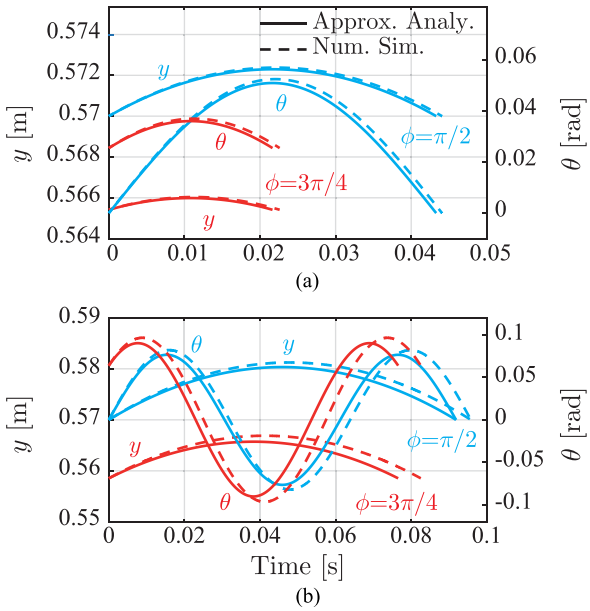

Fig. 2. Periodic solutions for $\phi = \pi/2$ (blue lines) and $\phi = 3\pi/4$ (red lines). (a) used $k_t = 500$ Nm/rad and $n = 1$, (b) used $k_t = 1000$ Nm/rad and $n = 2$.

original nonlinear equations and conditions (1), (2), and (3), and obtained periodic solutions numerically using the Newton-Raphson method. Fig. 2 compares the periodic solutions for $\phi = \pi/2$ and $\phi = 3\pi/4$, where Fig. 2(a) used $k_t = 500$ Nm/rad and $n = 1$, and Fig. 2(b) used $k_t = 1000$ Nm/rad and $n = 2$. The approximate periodic solutions are similar to the periodic solutions obtained by numerical simulations.

C. Dependence of Locomotion Factors on Torsional Spring Constant

The periodic solution (17) depends on the torsional spring constant k_t. The mechanical energy E and the apex height h are given by

$$\begin{aligned} E &= m(\dot{y}^*(0))^2 + J(\dot{\theta}^*(0))^2 + 2mgy^*(0) + 2k_t(\theta^*(0))^2 \\ &= 2mgy^*(T/2) + 2k_t(\theta^*(T/2))^2 \\ &= \frac{mg^2}{\omega^2}\left\{\left(1 + \frac{mL^2}{J} + \frac{mL^2}{J\tan^2\phi}\right)(n\pi - \phi)^2 \right. \\ &\quad \left. + \frac{2mL^2}{J\tan\phi}(n\pi - \phi)\right\} + 2mgl, \end{aligned} \tag{18}$$

$$h = y^*(T/2) = \frac{g(n\pi - \phi)^2}{2\omega^2} + \frac{mgL^2(n\pi - \phi)}{J\omega^2\tan\phi} + l. \tag{19}$$

The impulse Δp at foot contact is given by

$$\begin{aligned} \Delta p &= 2m(\dot{y}^*(0) - \dot{y}^*(T)) = 4m\dot{y}^*(0) \\ &= 2mgT = \frac{4mg(n\pi - \phi)}{\omega}. \end{aligned} \tag{20}$$

It can also be written using h in (19) by

$$\Delta p = 4m\sqrt{g(h - y^*(0))}, \tag{21}$$

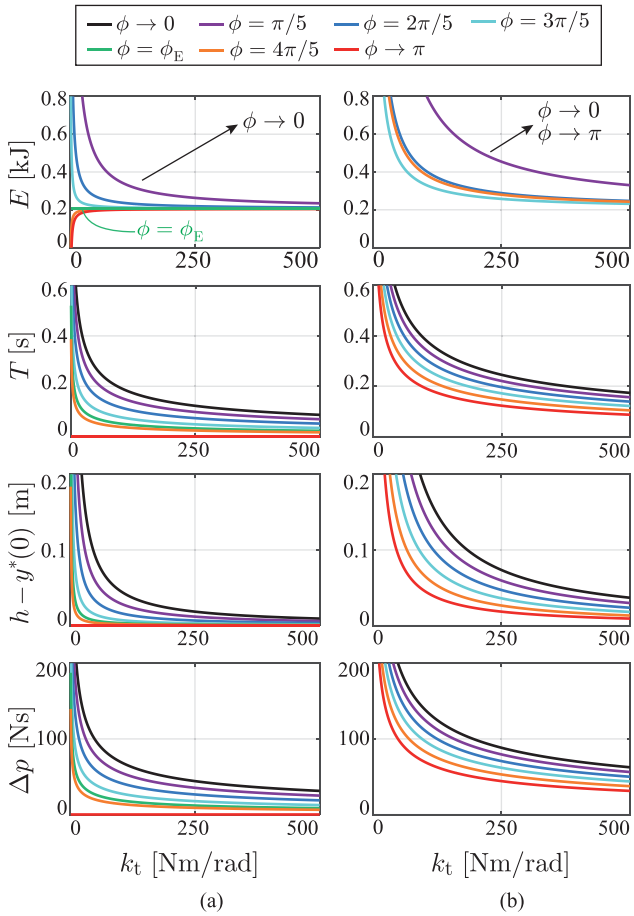

Fig. 3. E, T, $h - y^*(0)$, and Δp of periodic solutions for k_t for (a) $n = 1$ and (b) $n = 2$. $\phi = \phi_E$ is used only for $n = 1$.

where $h - y^*(0) = g(n\pi - \phi)^2/(2\omega^2) = gT^2/8$. Because we assumed infinitesimal stance phases, impulses at foot contact reflect the dynamical effect from the ground. Therefore, we focused on impulse instead of GRF, particularly in the next section.

Fig. 3 shows E, T, $h - y^*(0)$, and Δp for k_t for (a) $n = 1$ and (b) $n = 2$. T, $h - y^*(0)$, and Δp decrease as k_t irrespective of ϕ, while E depends on ϕ. Specifically, when $n = 1$, E monotonically decreases for $\phi < \phi_E$ and increases for $\phi > \phi_E$ as k_t (E diverges to infinity when ϕ approaches 0, and it decreases and approaches the red line in Fig. 3(a) as ϕ approaches π), where $\phi_E (\sim 2.3)$ is obtained from (18) by

$$\left(1 + \frac{mL^2}{J} + \frac{mL^2}{J\tan\phi_E}\right)(\pi - \phi_E) + \frac{2mL^2}{J\tan\phi_E} = 0. \tag{22}$$

When $n = 2$, E monotonically decreases as k_t (E decreases and increases depending on ϕ and it diverges to infinity when ϕ approaches 0 or π).

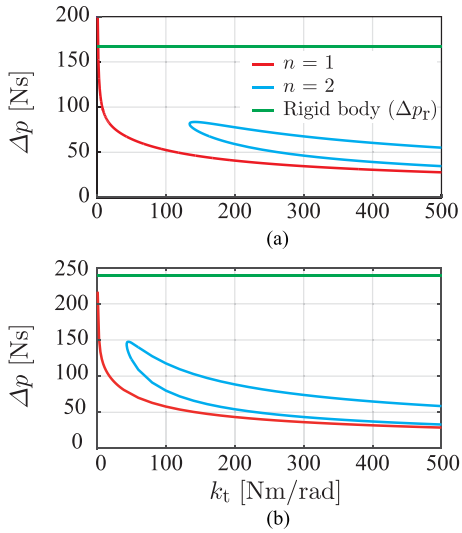

Fig. 4. Δp for $k_{\rm t}$ for (a) $E = 300$ J and (b) $E = 400$ J. Horizontal green line shows impulse $\Delta p_{\rm r}$ of rigid body model (described in Section IV-B).

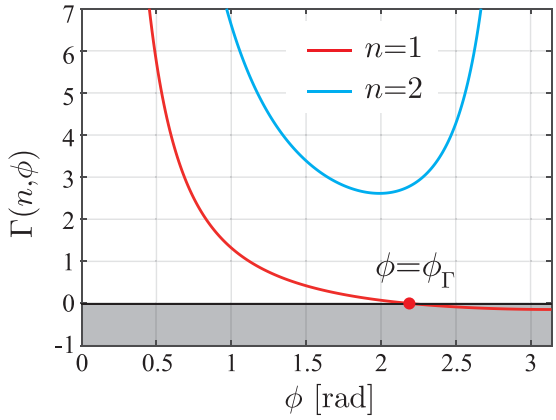

Fig. 5. $\Gamma(n,\phi)$ for $k_{\rm t} = 200$ Nm/rad. When $\Gamma > 0$, impulse of rigid body model is greater than that of flexible body model. When $\Gamma < 0$, impulse of rigid body is less than that of flexible body model.

IV. Impulse

Here, we investigated the contribution of body flexibility to foot loading using the approximate periodic solutions of the simple analytical model obtained in the previous section.

A. Dependence of Impulse on Torsional Spring Constant

Our previous study [24] revealed that the maximum GRF in bounding gait decreased as the torsional spring constant increased when the mechanical energy was identical. To clarify this mechanism using our simplified model, we recalculated the relationship between the impulse Δp and the torsional spring constant $k_{\rm t}$ of the simple analytical model by fixing the mechanical energy E.

Fig. 4 shows Δp for $k_{\rm t}$ for (a) $E = 300$ J and (b) $E = 400$ J. Δp is uniquely determined for $k_{\rm t}$ for $n = 1$, while it is not unique for $n = 2$, for the following reason. When E and n are given, ϕ is determined from $k_{\rm t}$. ϕ is unique for $n = 1$ because E monotonically decreases as ϕ, as shown in Fig. 3(a). In contrast, ϕ is not unique for $n = 2$ because E decreases or increases depending on ϕ, as shown in Fig. 3(b) and different values of ϕ have the same E. Regardless of E or n, Δp decreases as $k_{\rm t}$. These results explain why the maximum GRF in bounding gait decreased as the stiffness of the flexible body joint increased in our previous study [24].

B. Comparison of Impulse With Rigid Body Model

Our previous study [24] also revealed that the maximum GRF in the bounding gait of a model with a flexible body joint was lower than that of a model without a flexible body joint. To clarify this mechanism, we used an additional physical model (rigid body model), in which the fore and hind bodies are combined into one rigid body, as in our previous study [24]. The physical configuration of the rigid body model is identical to that of the model in Fig. 1(b) (the flexible body model) except for the torsional spring joint. Under the same movement constraints as the flexible body model, the state variables for the rigid body model can be described by the vertical position of the COM of the model $y_{\rm r}$ and the velocity $\dot{y}_{\rm r}$. The mechanical energy is given by $E_{\rm r} = m(\dot{y}_{\rm r}^*(0))^2 + 2mgy_{\rm r}^*(0)$ and the impulse is given by $\Delta p_{\rm r} = 4m\dot{y}_{\rm r}^*(0)$ for the periodic solution $y_{\rm r}^*(t)$. We compared the impulse between the flexible and rigid body models below when their mechanical energies were identical (for $E_{\rm r} = 300$ J and 400 J, the comparison is shown in Fig. 4).

From $E = E_{\rm r}$, $y_{\rm r}^*(0) = l$, and (18), we obtain

$$m(\dot{y}_{\rm r}^*(0))^2 - m(\dot{y}^*(0))^2 = J(\dot{\theta}^*(0))^2 + 2k_{\rm t}(\theta^*(0))^2 - 2mg(y^*(0) - l). \tag{23}$$

Therefore, when the following condition is satisfied for the function $\Gamma(n,\phi)$, $\dot{y}_{\rm r}^*(0) > \dot{y}^*(0)$ is satisfied and the impulse of the flexible body model is less than that of the rigid body model:

$$\begin{aligned}\Gamma(n,\phi) &= J(\dot{\theta}^*(0))^2 + 2k_{\rm t}(\theta^*(0))^2 - 2mg(y^*(0) - l) \\ &= \frac{m^2g^2L^2}{J\omega^2}\left\{\left(1 + \frac{1}{\tan^2\phi}\right)(n\pi - \phi)^2 \right. \\ &\quad \left. + \frac{2}{\tan\phi}(n\pi - \phi)\right\} > 0.\end{aligned} \tag{24}$$

The sign of $\Gamma(n,\phi)$ is determined only by n and ϕ and is independent of $k_{\rm t}$. Fig. 5 shows $\Gamma(n,\phi)$ for $n = 1$ and $n = 2$ with $k_{\rm t} = 200$ Nm/rad. While $\Gamma(n,\phi) > 0$ is always satisfied for $n = 2$, $\Gamma(n,\phi) > 0$ is satisfied for $n = 1$ for $\phi < \phi_\Gamma$, where $\phi_\Gamma\,(\sim 2.2)$ is obtained from (24) by

$$\Gamma(1,\phi_\Gamma) = 0. \tag{25}$$

However, when $\phi > \phi_\Gamma\,(\sim \phi_{\rm E}$ in Fig. 3(a)), the region of $(E, k_{\rm t})$ is extremely limited and induces notably small $k_{\rm t}$ and T, as shown in Fig. 3(a). This solution is singular and produces an unusual bounding gait. Therefore, most periodic solutions satisfy $\phi < \phi_\Gamma$ and $\Gamma > 0$. These results explain why the flexible body model exhibited smaller maximum GRF than the rigid body model in our previous study [24].

To further elucidate why the model with a flexible body joint exhibits smaller maximum GRF than the model without a flexible body joint, while a stiffer body exhibits smaller maximum GRF than a highly flexible body, we examined a case in which the stiffness of the flexible body model approached infinity, and compared the results with those of the rigid body model. When n is finite and $k_{\rm t} \to \infty$,

$$T \to 0 \tag{26}$$

is satisfied as shown in Fig. 3. This indicates that the model does not move and $\Delta p \to 0$. This is different from the movement of the rigid body model.

Although this may differ from animal movement, we also increased n as $k_{\rm t}$. For $\omega = \sqrt{2k_{\rm t}/J}$, we increased n and $k_{\rm t}$ under the condition $\lim_{\omega,n\to\infty} n/\omega = \alpha(>0)$ to avoid $T \to 0$. From (17), we obtain $T \to 2\pi\alpha$ and

$$y^*_\infty(t) = -\frac{g}{2}t^2 + g\pi\alpha t + l, \tag{27a}$$

$$\dot{y}^*_\infty(t) = -gt + g\pi\alpha, \tag{27b}$$

$$\theta^*_\infty(t) = 0, \tag{27c}$$

$$\dot{\theta}^*_\infty(t) = \frac{mgL\pi\alpha}{J\sin\phi}\sin\omega t, \tag{27d}$$

where $X_\infty(t) = \lim_{\omega,n\to\infty} X(t)$. When the mechanical energy is identical between the flexible and rigid body models, from (18) we achieve

$$\frac{J+mL^2}{J}mg^2\pi^2\alpha^2 + 2mgl = m(\dot{y}_{\rm r}(0))^2 + 2mgl. \tag{28}$$

It yields

$$\dot{y}^*_\infty(0) = \sqrt{\frac{J}{J+mL^2}}\dot{y}_{\rm r}(0) < \dot{y}_{\rm r}(0) \tag{29}$$

and

$$\Delta p_\infty < \Delta p_{\rm r}. \tag{30}$$

This implies that even when the body spring of the flexible body model is infinitely stiff, the movement of the flexible body model is different from that of the rigid body model and the impulse of the flexible body model is lower than that of the rigid body model.

C. Comparison of Impulse With Bounding Gait Model

In the approximate analysis, we constrained the flexible body model so that it moves only vertically and foot contact occurs instantaneously and simultaneously between fore and hind legs to clarify the effects of body flexibility on foot loading in quadruped bounding. To verify whether our findings remained significant even without these constraints, we performed numerical simulations of the original model in Fig. 1(a) (bounding gait model) used in [24]. This model included horizontal movement and included leg springs. The foot contact did not necessarily occur simultaneously between the fore and hind legs. We compared the body flexibility effects on foot loading between the approximate analysis of the flexible body model and this numerical simulation. Because the bounding gait model receives not only vertical GRF but also horizontal GRF during the stance phase by the leg springs, we calculated the impulse from the GRFs to compare the simulation results with the analytical results of the flexible body model.

To find periodic solutions of the bounding gait model, we defined the Poincaré section at the apex height of the COM of the whole body. We set $t = 0$ at the apex height. We assumed that both legs would have to experience the stance phase once before the intersection with the Poincaré section and that the trunk joint oscillated only once. We neglected the horizontal position because it monotonically increases during locomotion and is not periodic. Based on the findings of Raibert [26], we assumed the constraints of movement by

$$\theta_2(0) = -\theta_1(0), \tag{31a}$$

$$\dot{\theta}_2(0) = \dot{\theta}_1(0), \tag{31b}$$

so that the whole body posture is symmetrical about a vertical axis through the body joint and that the body spring is fully bent at the apex height. We fixed the horizontal velocity of the COM of the whole body $\dot{x}_{\rm c}(0)$ and the pitch angle velocity $\dot{\theta}_1(0)$. The mechanical energy $E_{\rm b}$ of the bounding gait model at the apex height is given by

$$E_{\rm b} = E_0 + m\dot{x}^2_{\rm c}(0) + (J + mL^2\cos^2\theta_1(0))(\dot{\theta}_1(0))^2, \tag{32}$$

where $E_0 = 2mgy_{\rm c}(0) + 2k_{\rm t}(\theta_1(0))^2$ and $x_{\rm c}$ and $y_{\rm c}$ are the horizontal and vertical positions, respectively, of the COM of the whole body. E_0 consists of the same terms as the mechanical energy E of the flexible body model, as shown in the second line of (18). We fixed values of E_0, $\dot{x}_{\rm c}(0)$, and $\dot{\theta}_1(0)$. We used a Poincaré map P denoted by

$$y_{{\rm c},n+1}(0) = P(y_{{\rm c},n}(0), \boldsymbol{u}), \tag{33}$$

where $y_{{\rm c},n}(0)$ is $y_{\rm c}$ at the nth intersection with the Poincaré section and $\boldsymbol{u} = [\gamma^{\rm td}_1\ \gamma^{\rm td}_2]$ is the parameter set. For a periodic gait, $y^*_{\rm c}(0) = P(y^*_{\rm c}(0), \boldsymbol{u}^*)$ is satisfied, where $y^*_{\rm c}(0)$ is a fixed point on the Poincaré section. We numerically searched fixed points for periodic bounding gaits using the function `fsolve` in MATLAB.

We found a hopping (in which the model moves only vertically and foot contact occurs simultaneously between fore and hind legs) by using $\dot{x}_{\rm c}(0) = 0.0$ m/s and $\dot{\theta}^*_1(0) = 0.0$ rad/s and bounding gaits (in which the model moves horizontally and foot contact occurs at different timings between fore and hind legs) by using (i) $\dot{x}_{\rm c}(0) = 0.5$ m/s and $\dot{\theta}^*_1(0) = -0.2$ rad/s and (ii) $\dot{x}_{\rm c}(0) = 1.0$ m/s and $\dot{\theta}^*_1(0) = -0.4$ rad/s. Fig. 6 shows the periodic solutions of the hopping and bounding gaits by using $k_{\rm t} = 250$ Nm/rad and $E_0 = 300$ J; (a) vertical position $y_{\rm c}$ and relative pitch angle $\theta_2 - \theta_1$ (this corresponds to 2θ of the flexible body model), (b) GRF. These solutions are normalized by gait cycle duration and 50% of the gait cycle indicates the apex height. The vertical position and pitch angle of the body show similar profiles to those of the flexible body model with $n = 1$ (Fig. 2(a)). The GRF of the hopping has a similar shape to that of the bounding gait, although the bounding gait has different foot-contact and lift-off timings between the fore and hind legs, unlike the hopping.

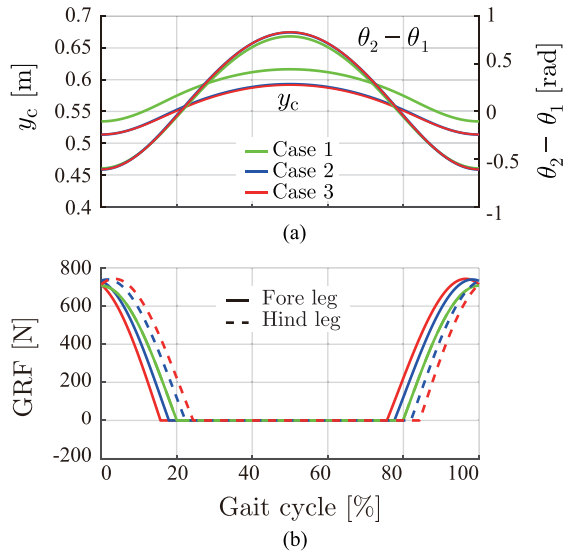

Fig. 6. Periodic solutions of bounding gait model normalized by the gait cycle duration for hopping (Case 1: $\dot{x}_c(0) = 0.0$ m/s and $\dot{\theta}_1(0) = 0.0$ rad/s, green line), and bounding gaits (Case 2: $\dot{x}_c(0) = 0.5$ m/s and $\dot{\theta}_1(0) = -0.2$ rad/s, blue line, and Case 3: $\dot{x}_c(0) = 1.0$ m/s and $\dot{\theta}_1(0) = -0.4$ rad/s, red line) using $k_t = 250$ Nm/rad and $E_0 = 300$ J. (a) shows y_c and $\theta_2 - \theta_1$, (b) shows GRF. 50% of the gait cycle indicates the apex height.

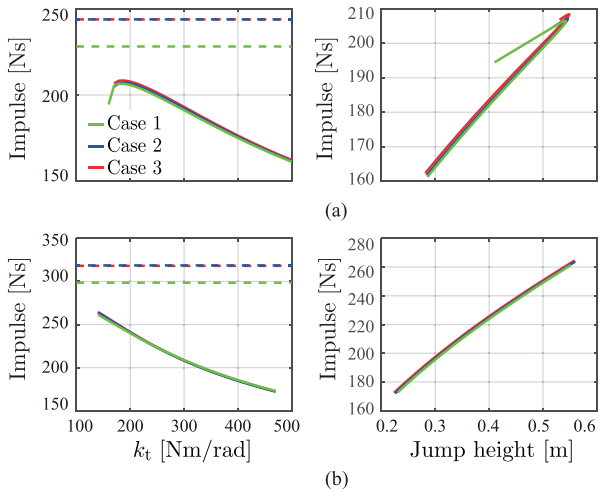

Fig. 7. Impulse for k_t and impulse for jumping height in a bounding gait model. (a) used $E_0 = 300$ J and (b) used $E_0 = 400$ J. The dotted line shows impulse of rigid body model. Case 1: $\dot{x}_c(0) = 0.0$ m/s and $\dot{\theta}_1(0) = 0.0$ rad/s, green line. Case 2: $\dot{x}_c(0) = 0.5$ m/s and $\dot{\theta}_1(0) = -0.2$ rad/s, blue line. Case 3: $\dot{x}_c(0) = 1.0$ m/s and $\dot{\theta}_1(0) = -0.4$ rad/s, red line.

To investigate the effects of body flexibility on foot loading, we found periodic solutions for hopping ($\dot{x}_c(0) = 0$ m/s, $\dot{\theta}_1(0) = 0$ rad/s) and bounding gaits ($\dot{x}_c(0) = 0.5$ m/s and $\dot{\theta}_1(0) = -0.2$ rad/s, $\dot{x}_c(0) = 1.0$ m/s and $\dot{\theta}_1(0) = -0.4$ rad/s) for various k_t. Fig. 7 shows the impulse of the obtained periodic solutions for k_t and the jump height $y_c(0) - \min(y_c(t))$ for (a) $E_0 = 300$ J and (b) $E_0 = 400$ J. The impulse generally decreases as k_t irrespective of $\dot{x}_c(0)$ nor E_0. These features are same as those in Fig. 4 obtained by the approximate analysis. Moreover, the impulse generally increased as the jump height. This is also consistent of the analytical solutions (21).

D. Application to Robots

Our previous study [24] revealed two important findings from the viewpoint of GRF; (i) introducing a flexible body joint reduced maximum GRF, and (ii) a stiffer body had a smaller maximum GRF than a highly flexible one. Although these findings seem to conflict with each other, our approximate analysis using a simplified model revealed that the two results were generally both correct, explaining why these apparently conflicting findings are observed in quadruped bounding.

The current findings suggest that it is beneficial for quadruped robots to contain a flexible body joint. In addition, stiffer bodies have smaller maximum GRF than highly flexible ones. However, the gait cycle duration decreases as the stiffness increases. Because actual robots are not completely passive and require actuators (e.g., to control the leg joint angles), body stiffness has limitations. Thus, there is a trade-off relationship between body stiffness and the properties of the actuators.

In the approximate analysis, we constrained the model so that it moved only vertically, and assumed infinitesimal stance phases and elastic collisions at foot contact. Although we verified the validity of our analysis by comparing our results with the numerical simulation results of the bounding gait model, the bounding model remains abstract because it is constrained in the sagittal plane and ignores fore-hind asymmetry in its physical properties. In future, we aim to incorporate these factors into our model to provide further guiding principles for the mechanical and control design of legged robots capable of fast locomotion.

V. Biological Relevance of Our Findings

During quadruped galloping in cheetahs, the animal extends and bends the spine only once in each gait cycle. This corresponds to $n = 1$ for the approximate periodic solution (17). As shown in Fig. 4, the impulse from the ground decreases as n decreases. This suggests that cheetahs determine their spine movement pattern to minimize foot loading while running.

In observational studies, the gait cycle duration of cheetahs has been reported to decrease as gait speed increases [25]. In the approximate solution (17), the gait cycle duration decreases as the torsional spring constant increases, as shown in Fig. 3. This suggests that the body stiffness needs to be increased to increase the gait speed in quadruped running, which is consistent with the suggestion by Koob and Long [27].

It has also been reported that the impulse on the legs in cheetahs decreases as the gait speed increases [25]. In the approximate solution, the impulse decreases as the torsional spring constant increases, as shown in Fig. 4. When the increase of the torsional spring constant corresponds to the increase of the gait speed as discussed above, our approximate analysis suggests that cheetahs reduce their gait cycle duration not only to achieve high speed, but also to decrease the impulse on the legs to avoid injury, similar to $n = 1$, as discussed above. Our results also suggest that the gait cycle duration is determined not only by leg movement but also by body flexibility, and that cheetahs control body flexibility to produce efficient running.

Although we investigated the contribution of body flexibility on foot loading by constraining some movements of our analytical model, our model has limited ability to fully clarify

the dynamic characteristics. In particular, galloping animals such as cheetahs utilize body flexibility not only to minimize foot loading, but also to increase stride length and enhance horizontal speed [1]. Moreover, trunk muscles are effectively used as actuators to produce a large amount of energy for acceleration. In addition, leg flexibility also contributes to effective gait and the relationship between the body and leg flexibilities is important. In future, we intend to improve our model to investigate these effects.

VI. Conclusion

In the current study, we constructed a simplified model by introducing physical constraints to our previous model, to clarify the dynamic roles of body flexibility in quadruped running. Approximate periodic solutions were derived by the linearization of the governing equations. We verified the validity of the approximate analysis by comparison with the original nonlinear model and our previous model bounding gait. Our approximate analysis clarified why maximum GRF values in the flexible body model were lower than those of the rigid body model, and why the maximum GRF values increased as body flexibility decreased in our previous study [24]. Furthermore, we discussed the biological relevance of our findings by comparing our results with previously reported observations in cheetahs. Specifically, our results suggest that cheetahs control body flexibility in accord with gait speed to decrease foot loading. Furthermore, we plan to develop quadruped robots that can perform fast running based on the findings of the approximate analysis in the current study.

Appendix
Foot Contact Dynamics

Here, we derive the relationship between the states immediately prior to and immediately following foot contact in the model. We assumed elastic collision for foot contact that involves no position change and energy conservation. We define Δp as the impulse at foot contact from the ground. Δp_x and Δp_y denote the impulses in horizontal and vertical directions, respectively. Δp_θ is the change in angular momentum caused by the impulse. Because the model is symmetrical between the fore and hind parts and the touchdown occurs simultaneously between the fore and the hind legs, Δp_x vanishes. The relationship of linear and angular momentum between immediately prior to and immediately following the collision gives

$$\Delta p_x = m(\dot{x}^+ - \dot{x}^-) = 0, \tag{34a}$$

$$\Delta p_y = m(\dot{y}^+ - \dot{y}^-) = \Delta p, \tag{34b}$$

$$\Delta p_\theta = J(\dot{\theta}^+ - \dot{\theta}^-) = \Delta p L \cos\theta. \tag{34c}$$

From energy conservation, we obtain

$$\frac{m}{2}((\dot{x}^+)^2 + (\dot{y}^+)^2) + \frac{J}{2}(\dot{\theta}^+)^2 = \frac{m}{2}((\dot{x}^-)^2 + (\dot{y}^-)^2) + \frac{J}{2}(\dot{\theta}^-)^2. \tag{35}$$

From (34) and (35), we obtain (3).

References

[1] M. Hildebrand, "Motions of the running cheetah and horse," *J. Mammal.*, vol. 40, no. 4, pp. 481–495, 1959.

[2] M. Hildebrand, "Further studies on locomotion of the cheetah," *J. Mammal.*, vol. 42, no. 1, pp. 84–91, 1961.

[3] M. Alexander, "Why mammals gallop," *Amer. Zoologist*, vol. 28, no. 1, pp. 237–245, 1988.

[4] R. Blickhan, "The spring-mass model for running and hopping," *J. Biomech.*, vol. 22, no. 11/12, pp. 1217–1227, 1989.

[5] T. McMahon and G. Cheng, "The mechanics of running: How does stiffness couple with speed?," *J. Biomech.*, vol. 23, no. 1, pp. 65–78, 1990.

[6] H. Geyer, A. Seyfarth, and R. Blickhan, "Spring-mass running: Simple approximate solution and application to gait stability," *J. Theor. Biol.*, vol. 232, no. 3, pp. 315–328, 2005.

[7] H. Geyer, A. Seyfarth, and R. Blickhan, "Compliant leg behaviour explains basic dynamics of walking and running," *Proc. Roy. Soc. B*, vol. 273, no. 1603, pp. 2861–2867, 2006.

[8] S. Lipfert, M. Günther, D. Renjewski, S. Grimmer, and A. Seyfarth, "A model-experiment comparison of system dynamics for human walking and running," *J. Theor. Biol.*, vol. 292, pp. 11–17, 2012.

[9] R. Full and D. Koditschek, "Templates and anchors: Neuromechanical hypotheses of legged locomotion on land," *J. Exp. Biol.*, vol. 202, no. 23, pp. 3325–3332, 1999.

[10] R. Blickhan and R. Full, "Similarity in multilegged locomotion: Bouncing like a monopode," *J. Comparative Physiol. A*, vol. 173, no. 5, pp. 509–517, 1993.

[11] C. Farley, J. Glasheen, and T. McMahon, "Running springs: Speed and animal size," *J. Exp. Biol.*, vol. 185, pp. 71–86, 1993.

[12] M. Tanase, Y. Ambe, S. Aoi, and F. Matsuno, "A galloping quadruped model using left-right asymmetry in touchdown angles," *J. Biomech.*, vol. 48, no. 12, pp. 3383–3389, 2015.

[13] C. Remy, K. Buffinton, and R. Siegwart, "Stability analysis of passive dynamic walking of quadrupeds," *Int. J. Robot. Res.*, vol. 29, no. 9, pp. 1173–1185, 2010.

[14] I. Poulakakis, J. Smith, and M. Buehler, "Modeling and experiments of untethered quadrupedal running with a bounding gait: The Scout II Robot," *Int. J. Robot. Res.*, vol. 24, no. 4, pp. 239–256, 2005.

[15] I. Poulakakis, E. Papadopoulos, and M. Buehler, "On the stability of the passive dynamics of quadrupedal running with a bounding gait," *Int. J. Robot. Res.*, vol. 25, no. 7, pp. 669–687, 2006.

[16] P. Nanua and K. Waldron, "Energy comparison between trot, bound, and gallop using a simple model," *J. Biomech. Eng.*, vol. 117, no. 4, pp. 466–473, 1995.

[17] K. Waldron and P. Csonka, "Analyzing bounding and galloping using simple models," *ASME J. Mech. Robot.*, vol. 1, no. 1, 2009, Art. no. 011002.

[18] Q. Cao and I. Poulakakis, "Quadrupedal bounding with a segmented flexible torso: Passive stability and feedback control," *Bioinspiration Biomimetics*, vol. 8, no. 4, 2013, Art. no. 046007.

[19] Q. Cao and I. Poulakakis, "On the energetics of quadrupedal bounding with and without torso," in *Proc. IEEE/RSJ Int. Conf. Intell. Robots Syst.*, 2014, pp. 4901–4906.

[20] R. Yamasaki, Y. Ambe, S. Aoi, and F. Matsuno, "Quadrupedal bounding with spring-damper body joint," in *Proc. IEEE/RSJ Int. Conf. Intell. Robots Syst.*, 2013, pp. 2345–2350.

[21] S. Pouya, M. Khodabakhsh, A. Spröwitz, and A. Ijspeert, "Spinal joint compliance and actuation in a simulated bounding quadruped robot," *Auton. Robots*, vol. 41, no. 2, pp. 437–452, 2017.

[22] C. Wang, T. Zhang, X. Wei, Y. Long, and S. Wang, "Dynamic characteristics and stability criterion of rotary galloping gait with an articulated passive spine joint," *Adv. Robot.*, vol. 31, no. 4, pp. 168–183, 2017.

[23] C. Farley and C. Taylor, "A mechanical trigger for the trot-gallop transition in horses," *Science*, vol. 253, no. 5017, pp. 306–308, 1991.

[24] T. Kamimura, Y. Ambe, S. Aoi, and F. Matsuno, "Body flexibility effects on foot loading based on quadruped bounding models," *Artif. Life Robot.*, vol. 20, no. 3, pp. 270–275, 2015.

[25] P. Hudson, S. Corr, and A. Wilson, "High speed galloping in the cheetah (Acinonyx jubatus) and the racing greyhound (Canis familiaris): Spatio-temporal and kinetic characteristics," *J. Exp. Biol.*, vol. 215, no. 14, pp. 2425–2434, 2012.

[26] M. Raibert, *Legged Robot That Balance*. Cambridge, MA, USA: MIT Press, 1986.

[27] T. Koob and J. Long, "The vertebrate body axis: Evolution and mechanical function," *Amer. Zoologist*, vol. 40, no. 1, pp. 1–18, 2000.